Title

Turbulent-driven low-frequency sheared E × B flows as the trigger for the H-mode transition

Journal

Nuclear Fusion, 53(7)

ISSN

0029-5515

Authors

Tynan, GR
Xu, M
Diamond, PH
et al.

Publication Date

2013-07-01

DOI

10.1088/0029-5515/53/7/073053

Peer reviewed

Presented at the 2012 IAEA FEC Conference, San Diego CA, Oct 2012
submitted to Nuclear Fusion, January 2013
Revised April 2013 Accepted for Publication June 2013

Turbulent-driven Low-frequency Sheared ExB flows as the Trigger for the H-mode Transition

G.R. Tynan[1], M. Xu[1], P.H. Diamond[1,2], J.A. Boedo[1], I. Cziegler[1], N. Fedorczak[1], P. Manz[1], K. Miki[2], S. Thakur[1], L. Schmitz[3], L. Zeng[3], E.J. Doyle[3], G.M. McKee[4], Z. Yan[4], G.S. Xu[5], B.N. Wan[5], H.Q. Wang[5], H.Y. Guo[5], J. Dong[6], K. Zhao[6], J. Cheng[6], W.Y. Hong[6], L.W. Yan[6]

[1]Center for Momentum Transport and Flow Organization, UCSD, La Jolla, CA USA
[2]WCI Center for Fusion Theory, NFRI, Daejeon, Rep. of Korea
[3]Department of Physics and Astronomy, UCLA, Los Angeles, CA, USA
[4]Department of Engineering Physics, University of Wisconsin, Madison WI, USA
[5]Chinese Academy of Sciences Institute of Plasma Physics, Hefei, Anhui, China
[6]Center for Fusion Science, Southwestern Institute of Physics, Chengdu, Sichuan, China

Corresponding author: gtynan@ucsd.edu

Abstract

Experiments on HL-2A, DIII-D and EAST show that turbulence just inside the last closed flux surface (LCFS) acts to reinforce existing sheared ExB flows in this region. This flow drive gets stronger as heating power is increased in L-mode, and leads to the development of a strong oscillating shear flow which can transition into the H-mode regime when the rate of energy transfer from the turbulence to the shear flow exceeds a threshold. These effects become compressed in time during an L-H transition, but the key role of turbulent flow drive during the transition is still observed. The results compare favorably with a reduced predator-prey type model.

Introduction Operation in the High Confinement mode (H-mode) is a key part of the baseline operating scenario for ITER. The development of a reliable physics-based macroscopic power threshold model for access to H-mode requires an understanding of the underlying mechanism that leads to the formation of the H-mode regime. Recent work has shown that an intermediate Limit Cycle Oscillation regime (LCO) (which is sometimes termed an intermediate or I-phase) can develop[1] during the transition to H-mode. The LCO is characterized by short period (<1msec) oscillations in both the turbulence amplitude and the sheared low-frequency (LF) poloidally/toroidally symmetric (m,n=0) $\mathbf{E}_r(t)\times\mathbf{B}_0$ flow denoted by $V_{ExB}^{LF}(t)=\left.\frac{E_r(t)\times B}{B^2}\right|_{m,n=0}$ in the region ~1-2cm inside the LCFS, and by variations in cross-field transport and divertor D_α light emissions. These dynamics co-exist with and include the slowly evolving (many msec to many 10's msec) m,n=0 ExB shear flow associated with the ion pressure gradient via the radial force balance, sometimes denoted as either the diamagnetic ExB flow, V_{dia}, or mean shear flow, V_{MSF}. These observations have been interpreted as being qualitatively consistent with a predator-prey model of the L-H transition[2]. However, to date no direct measurement of the development and evolution of the key physics quantity in this model –the Reynolds stress mediated transfer of turbulent kinetic energy to $V_{ExB}^{LF}(t)$, also known as the power transfer or shear flow energy production $P_{LF}=\langle\tilde{v}_r\tilde{v}_\theta\rangle\frac{\partial V_{ExB}^{LF}}{\partial r}$ - have been made in strongly heated L-modes, in the LCO or during the H-mode transition. This paper provides such results from work in the HL-2A, DIII-D and EAST tokamak devices. The results provide significant support for the predator-prey model, suggesting a pathway to a physics-based understanding of the L-H transition.

Theoretical Background: The evolution of the turbulent and m,n=0 sheared ExB flow kinetic energies, denoted $\left\langle \tilde{v}_{\perp}^{2} \right\rangle$ and $V_{ExB}^{LF^2}$ respectively, can be viewed as a simple power balance between the turbulent scale and the zonal flow scale. Due to pressure gradient-driven instabilities, fluctuation power is input into the finite (m,n) turbulence scales from the pressure gradient which acts as a free energy source. Some of this power is transferred to small spatial scales (i.e. high frequency/high wavenumber) and some into the m,n=0 sheared flows where it is then dissipated by viscous or flow-damping mechanisms respectively. The power balance for the turbulent scale and m,n=0 shear flow scales can then be written in terms of two equations:

$$\frac{\partial \left\langle \tilde{v}^{2} \right\rangle}{\partial t} = \left(\gamma_{eff} - \gamma_{decorr}^{pl} \right) \left\langle \tilde{v}^{2} \right\rangle - P_{LF}$$

$$\frac{\partial}{\partial t} \left\langle V_{ExB}^{LF^2} \right\rangle = P_{LF} - \gamma_{ZF} \left\langle V_{ExB}^{LF^2} \right\rangle$$

where the effective turbulence energy input rate is given by $\gamma_{eff} = \gamma_{eff}(\nabla n, \nabla T, V_E', ...)$, the m,n=0 ExB flow damping rate is given by γ_{LF}, and the plasma-frame decorrelation rate by γ_{decorr}^{pl}, indicating the rate of nonlinear energy transfer to the high k region where viscous dissipation occurs. The power transfer or production term P_{LF} has already been introduced above, and appears as a sink in the first equation and a source in the second equation. We note that this simple power balance model for the turbulence/sheared ExB system reduces to the published predator-prey model[2] if the input rate is given as $\gamma_{eff} = \frac{\gamma_l}{1 + \alpha V_{MSF}'^2}$ where $\gamma_l = \gamma_l \left(\nabla n, \nabla T_{i,e} \right)$ is the linear growth rate of the gradient-driven instability in the

absence of flow shear, the pressure gradient is given as $\nabla p_i \propto q_i$ where the control parameter q_i denotes the heat flux through the system, the mean shear flow is proportional to the curvature of the pressure profile, i.e. $V'_{MSF} \propto p_i''$, the stress is taken to scale as $\langle \tilde{v}_r \tilde{v}_\theta \rangle \propto V'_E$ and α is a constant parameter. Estimates for γ_{eff} can be obtained from measurements of $\frac{1}{\tilde{v}_\perp^2}\frac{\partial \tilde{v}_\perp^2}{\partial t}, \gamma_{decorr}^{pl}$ and $\langle \tilde{v}_r \tilde{v}_\theta \rangle' V_{ExB}^{LF}$, or it can be modeled. The production term P_{LF} is determined via an approach similar to that used in earlier work[3] in which the relevant quantities are computed in the time-domain using suitably filtered and averaged quantities. This approach implicitly assumes that there is a separation of timescales (or equivalently frequency) between the turbulent and m,n=0 sheared ExB flow scales, which in turn requires *a priori* knowledge of the relevant timescales. For the HL-2A, EAST and DIII-D devices these scales have previously been identified (see e.g. [4-6]). We also point out that this zero-dimensional model neglects the divergence of triple product terms in the energy balance model equations[7] which correspond to turbulence amplitude spreading and turbulent scattering of shear flow; the significance of these terms are the focus of current work.

.

Model Behaviors: When $0 < P_{LF} < \gamma_{ZF} \langle V_{ZF}^2 \rangle$ this system has a fixed point solution given approximately as $V_{ExB}^{LF} \approx \left[\frac{\left(\gamma_{eff} - \gamma_{decorr}^{pl}\right)}{\gamma_{LF}} \langle \tilde{v}_\perp^2 \rangle \right]^{1/2}$. A slow increase in the heat flux (e.g. slow enough so that the edge gradients evolution is slow compared to the confinement time) should then increase the density and temperature gradients and heat the edge, resulting in an increase in the turbulence amplitude and a decreased rate of zonal flow

damping γ_{LF}. As a result $\tilde{v}_\perp^2$, $V_{ExB}'^{LF}$ and P_{LF} should grow with increased heating power in fixed point L-mode conditions. We note that recent studies in L-mode discharges have confirmed this behavior[8]. When $P_{LF} > \gamma_{LF} V_{ExB}^{LF^2}$, a growing solution $\frac{\partial V_{ExB}^{LF^2}}{\partial t} > 0$ can now exist and thus $V_{ExB}^{LF^2}$ can begin to grow at the expense of the turbulent energy $\tilde{v}_\perp^2$, signaling the onset of the LCO regime. If the energy transfer rate becomes strong enough so that $P_{LF} > \left(\gamma_{eff} - \gamma_{decorr}\right)\left\langle \tilde{v}_\perp^2 \right\rangle$, then the turbulence amplitude (and thus the turbulent-driven cross-field transport) can collapse, resulting in a quenching of turbulent transport and an increase in the ion pressure gradient and the MSF. As noted above, in the predator-prey model the effective energy input rate is decreased by the mean shear flow, i.e. $\gamma_{eff} = \frac{\gamma_l}{1 + \alpha V_{MSF}'^2}$. As a result, as the MSF builds up during the LCO regime, the energy input rate into the turbulence gradually decreases. With sufficiently strong MSF, the turbulent energy never recovers after the peak in the turbulent-driven LF ExB shear flow energy. Instead the turbulence energy decays away and a regime of strong steady-state MSF with correspondingly large pressure gradient develops, signaling the onset of the H-mode regime.

When the heating power is sufficiently strong, the above sequence is compressed into a short (~1msec) transient event in which the gradients and associated mean shear flow increases. The turbulent-driven zonal flow then undergoes a rapid growth and for a short period (~10^{-2} a/C_S~1msec) (here a denotes the minor radius and C_S the ion acoustic speed) succeeds in transferring nearly all of the turbulent energy into the low-frequency shear flow. As a result cross-field transport collapses,

the gradients increase rapidly and a strong mean shear flow is then locked in. The details of these model dynamics have recently been published[9], and the interested reader is referred to that paper for further discussions. As shown below, experiments show these key signatures, providing support that the underlying predator-prey model captures the essential elements of the transition to H-mode.

Experiments: We have performed experiments to test these expectations in the HL-2A, EAST and DIII-D tokamaks. Suitably arranged multi-tipped Langmuir probe arrays (see e.g. [10]) are used to measure the radial profiles and time-evolution of the turbulent stress, turbulence energy, LF ExB flow, plasma frame decorrelation rate, and turbulence recovery rate in the region slightly (~1cm) inside the LCFS. In DIII-D, other diagnostics (e.g. Doppler Backscattering (DBS) and Beam Emission Spectroscopy (BES) are used to cross-check the probe measurements when possible. As noted earlier, the m,n=0 nature of the low-frequency ExB flows is confirmed with poloidally and toroidally separated multipoint probe or DBS measurements; these flows are also found to exhibit a low frequency nature (i.e. their frequency is at or below the characteristic frequencies of the geodesic acoustic mode (GAM) at ~C_s/R~10-15kHz), well separated from the higher frequency broadband fluctuations that characteristically have a peak frequency in the range of 50-100kHz with a broad power-law decay ~ $1/f^{\alpha}$ where α>1 for higher frequencies.

Fixed-point L-mode: In HL-2A a series of time-stationary inner-wall limited discharges with a variety of ECH heating powers are used to examine turbulence-ZF energy transfer[8] in steady-state L-mode discharges. The required multipoint turbulence measurements are obtained in the region just inside the LCFS in Ohmically heated and ECH heated

discharges, and the frequency-resolved energy transfer is then inferred using established techniques[8] yielding two-dimensional bispectral measurements of energy transfer across frequency scales. These bispectra can then be integrated over one frequency axis to yield the net energy transfer into/out of a particular frequency f. The frequency resolved net energy transfer is shown in Fig. 1 below for the case of a 700kW ECH heated discharge. The results show that turbulent kinetic energy is transferred out of intermediate (20-50 kHz) frequencies and into both low-frequency (<15kHz) flcutuations previously identified as m,n=0 sheared ExB flows, as well as into higher frequency (>50kHz) ranges (Fig. 1). The cited work shows that this transfer process gets more pronounced with increased ECH heating. These observations support the notion that the two-scale power balance model described above (and which underpins the predator-prey model of the L-H transition) has a basis in experimental observation.

Additional insight into this physics can be obtained by considering radial profiles of the Reynolds force $F_{\theta_{\mathrm{Re}y}} = -\dfrac{\partial\langle \tilde{v}_r \tilde{v}_\theta \rangle}{\partial r}$, the low frequency ExB flow V_{ExB}^{LF} and the product of these two, P_{Re} ,which is equal to the rate of work done by the turbulence on the low frequency ExB flow which in a 0-D model satisfies $P_{\mathrm{Re}} = P_{LF}$. The Reynolds stress is computed using a time-domain high-pass digital filter to isolate velocity fluctuations with f>20kHz; the product of these fluctuations is then time averaged to produce the $F_{\theta_{\mathrm{Re}y}}$ (left panel). The low frequency ExB shear flow is computed from the radial gradient of the time-averaged plasma potential (center) and P_{Re} is then computed from the product of the first two results. We show results for Ohmic (black curves) 380 kW ECH (blue curves) and 730 kW ECH (read curves) heated discharges . The results clearly show that in these

time stationary L-mode discharges the Reynolds force acts to reinforce the ExB flow, and as a result the turbulence transfers energy into the large-scale shear flow consistent with the model expectations for fixed point L-mode behavior. Furthermore the Reynolds force, the magnitude of the shear flow, and the production term all increase substantially as the heating power is increased. These results show that the turbulence is acting to reinforce or amplify the shear flow at the boundary, and that this effect becomes stronger as the heating power is raised. The predator-prey model would then predict that when the transfer rate exceeds γ_{LF}, then V_{ExB}^{LF} can grow to much larger amplitudes and extract a significant fraction of energy from the turbulence. Without knowledge of this damping rate, we cannot test this prediction in the HL-2A data. However, experiments in DIII-D (discussed next) do allow us to examine these expectations in a more quantitative manner.

Transition to LCO or I-phase regime: The transition to LCO behavior is studied in DIII-D LSN discharges. The midplane fast scanning probe is inserted during the L-mode, is stationary approximately 1cm inside the LCFS while it captures the L-I transition, and then is retracted in the early (~10msec) I-phase. The resulting time resolved measurements just inside the LCFS (Fig. 3) then permit us to study the evolution of the power transfer into the m,n=0 shear flow during the onset of the LCO regime. The results show that V_{ExB}^{LF} begins to increase slightly (few 100's of μsec) before the oscillations in divertor D_α light (which are characteristic of the LCO regime) begin (Fig. 3a-b). The time required for parallel plasma propagation along the field lines can introduce a slight (~100-200 microsec) delay between the V_{ExB}^{LF} oscillations and the divertor D_α light oscillations, and thus this slight delay may reflect the time needed for parallel transport processes to begin to modulate

plasma particle input into the divertor due to modulations of cross-field tranpsort. A comparison of the rate of energy transfer, $P_{LF}/\tilde{v}_{\perp}^2$ and the plasma frame turbulent decorrelation rate γ_{decorr}^{pl} provides important insights into the physics of the onset of the LCO or I-phase regime. Here the ratio $P_{LF}/\tilde{v}_{\perp}^2$ provides a measure of the effective rate of energy transfer from the turbulent frequency range into the m,n=0 shear flow. The rate γ_{decorr}^{pl} is computed from the measured laboratory frame decorrelation rate $\gamma_{decorr}\big|_{lab}$, the measured poloidal decorrelation length L_{θ}^{corr}, and the measured low frequency ExB drift velocity V_{ExB}^{LF} via the relation $\gamma_{decorr}^{pl^2} = \gamma_{decorr}^2\big|_{lab} - \left(V_{ExB}^{LF}/L_{\theta}^{corr}\right)^2$. The results (Fig. 3 lower panel) show that in the fixed point L-mode regime, just before the transition to LCO regime, the turbulence has $\gamma_{decorr}^{pl} \approx P_{LF}/\tilde{v}_{\perp}^2 \approx 2-4\times10^5\,\mathrm{sec}^{-1}$, indicating that turbulent energy is dissipated to both low-frequency ExB flows and to high frequency, high wavenumber (and thus presumably viscous) dissipation processes at comparable rates. Furthermore, because the L-mode state is time-stationary, we can estimate that in L-mode just prior to entry into the LCO regime, the net rate of energy input into the turbulence must balance these combined dissipation processes, and thus we can estimate the effective energy input rate in L-mode as $\gamma_{eff}\big|_L = \gamma_{decorr} + P_{LF}/\left\langle\tilde{v}_{\perp}^2\right\rangle \approx 6-8\times10^5\,\mathrm{sec}^{-1}$. Examining the magnitudes of the stress and ExB flow in Lmode, we can also estimate $\gamma_{LF} \sim 10^5\,\mathrm{sec}^{-1}$.

The transition to the LCO state is observed to occur at about 1.6062 seconds as seen by the onset of oscillations in the data in Fig. 3. In the short (few 100 $\mu\,\mathrm{sec}$) time

period of the onset of the LCO phase, it seems unlikely that the mean density and temperature profiles would be able to evolve. Thus the free energy source driving the turbulence and the (m,n=0) flow damping rate γ_{LF} will remain roughly constant across the transition into the LCO state. Examining the results in Figure 3c, we note that at the onset of the LCO regime, the $P_{ZF}/\tilde{v}_{\perp}^2$ channel increases by a factor of ~2-3 to a value of about 10^6 sec^{-1} or so at 1.606 seconds while the decorrelation rate shows no similar prompt jump. Clearly then $P_{ZF}/\tilde{v}_{\perp}^2$ becomes the *dominant* turbulent energy dissipation channel as the LCO regime is entered. As a result, changes in V_{ExB}^{LF} can have a significant impact on the turbulent energy balance via the model equations given above.

Direct Evidence that Turbulent Stress Drives the m,n=0 Sheared ExB Flow: The above results are consistent with an interpretation that the time-varying shear flow in the LCO regime is in fact driven by the turbulence. Further supporting evidence can be found by an examination of the time-variation of the turbulent stress, turbulent energy and ExB shear flow during the LCO phase. Fig. 4 presents a detailed examination of these quantities obtained from probe measurements taken ~1cm inside the LCFS during a DIII-D LCO discharge. The stress and turbulent energy both grow as the m,n=0 ExB flow approaches its minimum value. Then, as the stress reaches its most negative value, the m,n=0 ExB flow begins to accelerate and reaches its maximum acceleration either just at or very shortly after the peak in the turbulent stress. Since the stress is nearly zero outside the LCFS, we can take the Reynolds force as being proportional to the value of the stress; thus stress

modulation represents a Reynolds force modulation. We therefore conclude that the stress can provide an acceleration which then modulates the m,n=0 ExB flow and that the observed flow dynamics are consistent with this interpretation.

We have also used BES turbulence imaging to study the power transfer evolution during the same L-mode to LCO transition. In particular, we have used velocimetry analysis[11, 12] of BES imaging data obtained *in the same discharges* to provide a similar calculation of the shearing rate and nonlinear power transfer rate during the L-mode to LCO transition. The results (Fig. 5) provide a qualitatively similar picture of the onset of strong nonlinear power transfer into the low frequency shear flow at the moment of the LCO transition, and a subsequent modulation in this transfer rate during the LCO regime. Thus these results do not seem to depend upon the use of probes to infer the results. We also note that radially resolved probe measurements show that these effects are localized to the region slightly (~1cm) inside the LCFS (Fig. 6).

LCO to H-mode transition: The radial profiles of V_{ExB}^{LF} and $\frac{\mathrm{P}_{LF}}{\left\langle \tilde{v}_{\perp}^{2} \right\rangle}$ obtained in L-mode, in early LCO phase, and in early (~10msec after onset) H-mode are shown in Fig. 6. The mean ExB velocity profile shows a weak shear layer in L-mode, and periods of significantly stronger flow in the LCO or I-phase regime. In the region inside the LCFS the ExB velocity shows large oscillations in the LCO regime, documented in detail above for the position ~-1cm inside the LCFS. In the H-mode, the ExB profile appears to "lock-in" the peak values found in the LCO or I-phase regime. In the LCO or I-phase regime, the transfer rate $P_{LF}/\tilde{v}_{\perp}^{2}$ increases markedly from L-mode values, and exhibits

large variations as the m,n=0 ExB flow and turbulence intensity oscillations occur. In H-mode, the power transfer rate then locks into values as large as those found in the intermediate LCO regime and equals or exceeds the effective energy input rate γ_{eff} from the free energy source.

L-H transition: The above results provide detailed insight into the L-LCO-H mode transition sequence. However, the question remains as to whether or not a similar physics picture is observed in a "normal" L-H transition that does not exhibit the intermediate LCO phase. We have performed experiments on the EAST device which provide an answer to this question. We used a single discharge that exhibited an L-LCO-H mode transition, went back into Lmode, and then had a normal L-H transition. The macroscopic parameters of the plasma were quite similar during these two transitions, allowing us to use results from the LCO regime in the analysis of the L-H transition. A detailed discussion of these results can be found in a recent paper[13].

Measurements of the rate of turbulence kinetic energy recovery $\frac{1}{\tilde{v}_\perp^2}\frac{\partial \tilde{v}_\perp^2}{\partial t}$ made in the LCO regime during periods when the zonal flow magnitude is negligible provide a direct experimental measurement of the net rate of energy input into the turbulence, i.e. of the quantity $\left(\gamma_{eff} - \gamma_{decorr}\right)$ which gives the net rate of energy input into the turbulence after accounting for transfer to high wavenumber scales where viscous dissipation occurs. These data are taken under conditions in which the edge gradients during the LCO regime and the L-H transition are the same to within the uncertainty of the measurements. The plasma in these experiments is therefore sitting very close to the threshold for the

transition to improved confinement. Multipoint probe measurements then provide a measure of P_{LF} during a "normal" L-H transition that does not exhibit an LCO phase but which otherwise has edge plasma gradients are nearly identical to those found during the LCO phase. Because the edge pressure gradients are similar, then presumably the net rate of energy input into the turbulence, $\gamma_{eff} - \gamma_{decorr}$ is unchanged going from the LCO to the L-H regimes. As a result, we can use the net rate of energy input $\gamma_{eff} - \gamma_{decorr}$ during the LCO regime to the study of the L-H transition. The ratio $P_{LF} \big/ \left(\gamma_{eff} - \gamma_{decorr}\right) \tilde{v}_{\perp}^2$ then indicates the ratio of the power transfer into the ZF normalized by the net power input into the turbulence. *Should this value exceed unity, then according to the model described above, the turbulent energy should drop significantly. The experimental results (Figure 7) show that this ratio does in fact peak near unity just before or at the drop in* D_α, which signifies the entrance into the H-mode regime. Thus just before an L-H transition the power transfer into the m,n=0 ExB flow becomes, momentarily at least, strong enough to transfer the turbulence energy to the flow at a rate faster than it can be input from the mean gradients, resulting in an observed turbulence collapse that is consistent with model expectations. Since cross field transport is caused by the turbulence, this collapse then leads to the build up of the edge gradients and associated mean shear flow. A detailed discussion of these observations and a comparison with predator-prey model results is available in the literature[12].

Comparison to predator-prey model: There are multiple points of agreement between the experimental observations and the predator prey model which is the motivation for

the power balance model described above. First the turbulence helps to sustain the m,n=0 ExB flow via a transfer of kinetic energy from the microscopic turbulence scale to the mesoscopic zonal flow scale, and growth of the ExB flow comes at the expense of the turbulent energy - which is an essential element of the predator-prey model. Second, the temporal relationship between turbulent stress and the sheared ExB drift is consistent with the model. Third, our experiments taken together with published work are consistent with the energy transfer in early LCO being associated with the turbulence-driven plasma flow, while later in the LCO regime and in H-mode the diamagnetic component of the m,n=0 ExB flow associated with grad-P_i (a.k.a. the MSF) becomes dominant[6]. Finally, the fast L-H transition appears to be a compressed version of this process in which a transient increase in turbulence-driven sheared ExB flow extracts nearly all the energy from the turbulence, which then collapses[13]. In particular, a detailed discussion of the predator-prey model predictions for both L-LCO-H mode and L-H transitions is also available[9]. Here we point out Figure 7 in this last reference, which provides an analogous plot of the evolution of turbulence energy, zonal flow and mean shear flow energy, and nonlinear energy transfer rate during an L-H transition. That result clearly shows the important role that the rate of energy transfer into the turbulent-driven sheared ExB flow (the "zonal flow" in the parlance of the predator-prey model) plays in initiating the L-H transition. Finally, although the EAST experiments do not yet have the requisite diagnostics, it is already well known that a strongly sheared ExB flow associated with a steep grad-P_{ion} can then develop at the H-mode transition, providing a mechanism to maintain the shear flow once the turbulent flow drive dies away after the onset of H-mode.

Summary & Conclusions: We find that the rate of Reynolds work done by turbulence on the mesoscale sheared m,n=0 ExB flows increases substantially as the L-mode heating power is increased due to an increase in the Reynolds force and in V_{ExB}^{LF} . At the transition to the LCO regime, the rate of energy transfer to the m,n=0 ExB flows, $P_{LF}/\left\langle \tilde{v}_{\perp}^{2} \right\rangle$, becomes 2-3 times larger than the plasma-frame turbulent decorrelation rate, γ_{decorr}^{pl}, and thus, for a fixed rate of energy input from the free energy source, will effectively govern the turbulence amplitude. This shows that the rate of m,n=0 flow drive then becomes the dominant turbulent energy sink in the LCO regime. Measurements ~1cm inside LCFS show that in the LCO regime, the turbulent kinetic energy $\left\langle \tilde{v}_{\perp}^{2} \right\rangle$, $V_{ExB}^{LF}(t)$ and Reynolds stress are strongly modulated in time, and the system can be considered to execute multiple orbits in a $\left\langle \tilde{v}_{\perp}^{2} \right\rangle$-$V_{ExB}^{LF^2}$ phase space. The peak Reynolds force is associated with the peak acceleration of $V_{ExB}^{LF}(t)$, and increases in $V_{ExB}^{LF^2}$ come at the expense of $\left\langle \tilde{v}_{\perp}^{2} \right\rangle$. We note that during the LCO, the shearing rate of $V_{ExB}^{\prime LF}$ is nearly equal to and tracks the variation of $P_{LF}/\left\langle \tilde{v}_{\perp}^{2} \right\rangle$, which suggests that the more commonly used shearing rate $V_{ExB}^{\prime LF}$ could actually be a measure of the rate of power transfer out of the turbulence and into the LF m,n=0 shear flows. As the LCO progresses, published work[6] shows that the diamagnetic ExB flow associated with ∇p_{ion} gradually increases to the point where $V_{dia}^{\prime}$ can maintain turbulence suppression. At the onset of H-mode the LCOs cease and the ExB shearing rate and power transfer lock into the strong flow shear and reduced turbulence and transport. During a rapid (i.e. a "normal") L-H

transition that does not exhibit an LCO regime, the power transfer is observed to transiently extract nearly all of the turbulence energy and transfer it into $V_{ExB}'^{LF}$, thereby quenching turbulent transport and allowing the steep gradients and mean shear flow associated with H-mode to then develop. These qualitative results compare favorably to a predator-prey model. Interestingly, we note that recent work in ALCATOR C-Mod shows that the Reynolds stress mediated power transfer from the fluctuations into the finite frequency geodesic acoustic modes also plays an important role in the onset of the I-mode[13]. Thus the nonlinear physics of turbulent-driven shear flows appears to play a key role in the formation of a number of types of improved confinement transitions in many devices.

There are several obvious next steps to take. First, experiments need to directly separate the evolution of the m,n=0 ExB into the ion pressure gradient and v x B components in order to clearly resolve the role of "zonal flows" and mean shear flows in this evolution, and a quantitative comparison with the predator-prey model should be done. Second, the understanding from this work should now be used to develop a macroscopic model of the L-H threshold that is based on microscopic physics. Third, we note that three dimensional effects may be important, motivating measurements of the other components of the turbulent stress matrix as was pointed out earlier by other workers[14]. Such work would then naturally link the L-LCO-H mode transition physics to the physics of intrinsic toroidal rotation. Finally, we note that these physics are essentially hydrodynamic processes, describable with fluid based models of the plasma that properly account for neoclassical flow damping and, perhaps, electromagnetic effects. Thus we can conclude that the L-H transition physics should be capable of being captured by suitable

turbulence-based simulations first using fluid and gyro-fluid models. These could be used to gain deeper insights into the physics that could eventually permit gyrokinetic-based simulations to then reproduce these dynamics.

Acknowledgements: This work was supported by the Natural Science Foundation of China, project number Nos. 11175060, 11075046 and 11175056, and by the National Magnetic Confinement Fusion Science Program of China under Contracts No. 2011GB107001 and 2010GB106008; by the U.S. Department of Energy (DOE) through Grant Numbers. DE-SC0001961, DE-FG02-08ER54984 ,DE-FG02-89ER53296, DE-FG02-08ER54999, DE-FG02-07ER54917, and DE-FC02-04ER54698; and by the WCI Program of the National Research Foundation of Korea funded by the Ministry of Education, Science and Technology of Korea [WCI 2009-001]. The authors would like to acknowledge the facilities, organizing Committee and participants of the Festival de Theorie, Aix en Provence, 2011 for stimulating discussions which helped motivate this work, and the work of the HL-2A, EAST and DIII-D teams for making these experiments possible.

References

1. T. Estrada, T. Happel, C. Hidalgo, E. Ascasibar and E. Blanco, Epl **92** (3) (2010).
2. E. J. Kim and P. H. Diamond, Phys. Rev. Lett. **90** (18) (2003).
3. E. Sanchez, C. Hidalgo, B. Goncalves, C. Silva, M. A. Pedrosa, M. Hron and K. Erents, J. Nucl. Mater. **337-39** (1-3), 296-300 (2005).
4. A. D. Liu, T. Lan, C. X. Yu, H. L. Zhao, L. W. Yan, W. Y. Hong, J. Q. Dong, K. J. Zhao, J. Qian, J. Cheng, X. R. Duan and Y. Liu, Phys. Rev. Lett. **103** (9) (2009).
5. K. J. Zhao, T. Lan, J. Q. Dong, L. W. Yan, W. Y. Hong, C. X. Yu, A. D. Liu, J. Qian, J. Cheng, D. L. Yu, Q. W. Yang, X. T. Ding, Y. Liu and C. H. Pan, Phys. Rev. Lett. **96** (25), 4 (2006).
6. L. Schmitz, Phys. Rev. Lett. **108** (2012).
7. P. Manz, M. Xu, N. Fedorczak, S. C. Thakur and G. R. Tynan, Phys. Plasmas **19** (1) (2012).
8. M. Xu, G. R. Tynan, P. H. Diamond, P. Manz, C. Holland, N. Fedorczak, S. C. Thakur, J. H. Yu, K. J. Zhao, J. Q. Dong, J. Cheng, W. Y. Hong, L. W. Yan, Q. W. Yang, X. M. Song, Y. Huang, L. Z. Cai, W. L. Zhong, Z. B. Shi, X. T. Ding, X. R. Duan, Y. Liu and H.-A. Team, Phys. Rev. Lett. **108** (24) (2012).
9. K. Miki, P. H. Diamond, O. D. Gurcan, G. R. Tynan, T. Estrada, L. Schmitz and G. S. Xu, Phys. Plasmas **19** (9) (2012).
10. M. Xu, G. R. Tynan, C. Holland, Z. Yan, S. H. Muller and J. H. Yu, Phys. Plasmas **16** (4) (2009).
11. C. Holland, G. R. Tynan, G. R. McKee and R. J. Fonck, Rev. Sci. Instrum. **75** (10), 4278-4280 (2004).
12. G. R. McKee, R. J. Fonck, D. K. Gupta, D. J. Schlossberg, M. W. Shafer, C. Holland and G. Tynan, Rev. Sci. Instrum. **75** (10), 3490-3492 (2004).
13. P. Manz, G. S. Xu, B. N. Wan, H. Q. Wang, H. Y. Guo, I. Cziegler, N. Fedorczak, C. Holland, S. H. Mueller, S. C. Thakur, M. Xu, K. Miki, P. H. Diamond and G. R. Tynan, Phys. Plasmas **19** (7) (2012).
14. B. Goncalves, C. Hidalgo, M. A. Pedrosa, R. O. Orozco, E. Sanchez and C. Silva, Phys. Rev. Lett. **96** (14), 4 (2006).

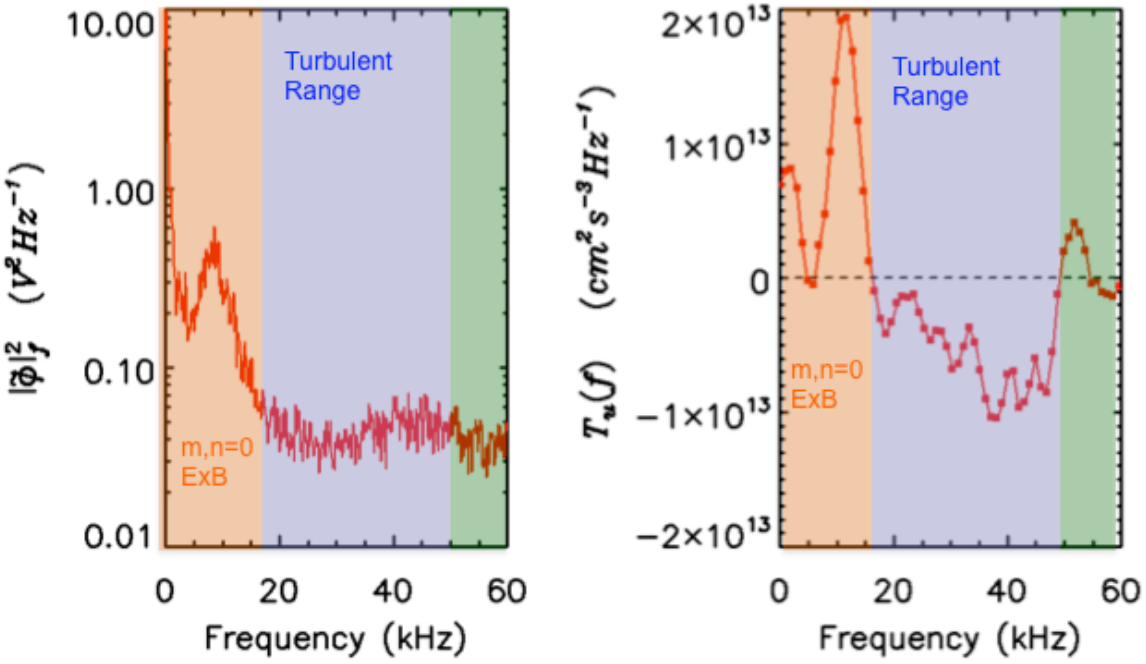

Fig. 1: Left: potential fluctuation spectrum; low-frequency m,n=0 ExB flow fluctuations (f<15kHz) turbulent frequency range (f>15kHz). Right: Frequency-resolved net kinetic energy transfer. Frequencies between ~15-50 kHz are losing energy to both higher frequencies (f>50kHz) and low frequencies (f<15kHz) associated with m,n=0 sheared ExB flows. The error bars on the kinetic energy transfer are estimated from the number of ensembles (N=300) to be +/-0.2x10^13 (cm^2/sec^3-Hz), consistent with the scatter in Fig.1 b.

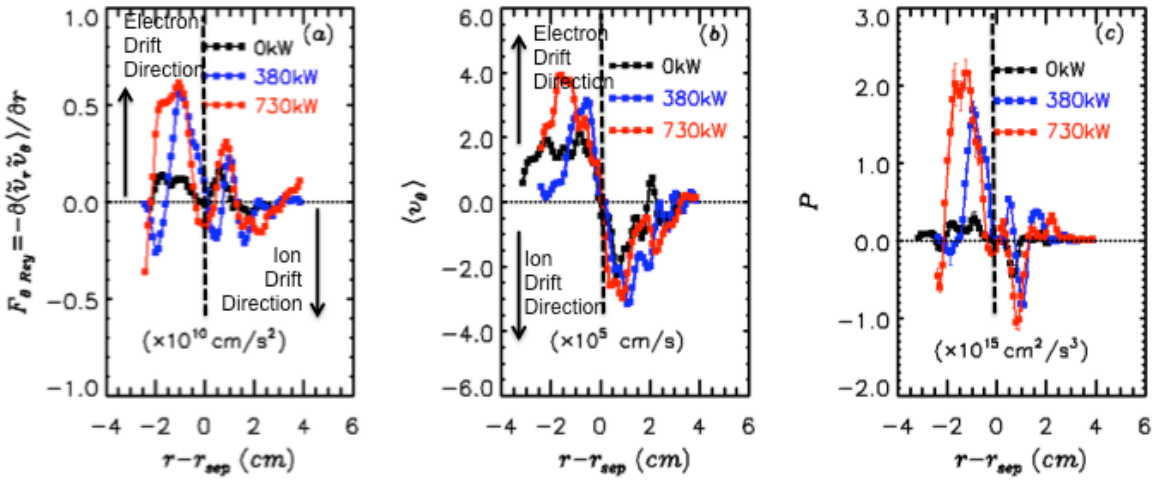

Fig. 2: Profiles of (a) Reynolds force, (b) <E>xB profiles (middle) and (c) rate of Reynolds work, P_{Re} for Ohmic (black), 380kW ECH heating (blue) and 730 kW ECH heating (red) discharges in HL-2A. Increased ECH heating results in an increased Reynolds force, an increased sheared ExB flow inside the LCFS and an increased P_{Re} which acts to reinforce the ExB flow in the region inside the LCFS.

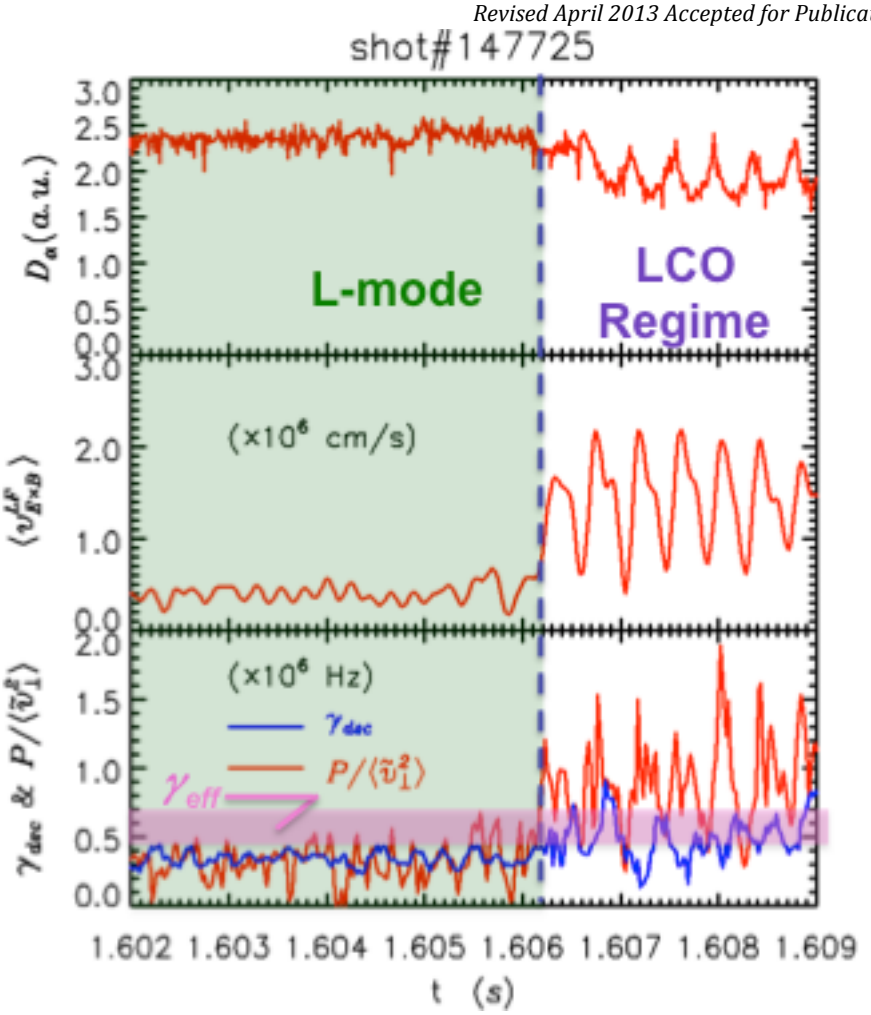

Fig. 3: (top) D_α light modulations; (middle) m,n=0 ExB flow velocity; (lower): plasma frame decorrelation rate (blue) and rate of energy transfer into m,n=0 ExB flow, $P_{LF}/\langle\tilde{v}_\perp^2\rangle$ (red). Energy transfer into m,n=0 ExB flows becomes the dominant turbulent energy loss channel in the LCO regime. Data obtained 1cm inside DIII-D LCFS.

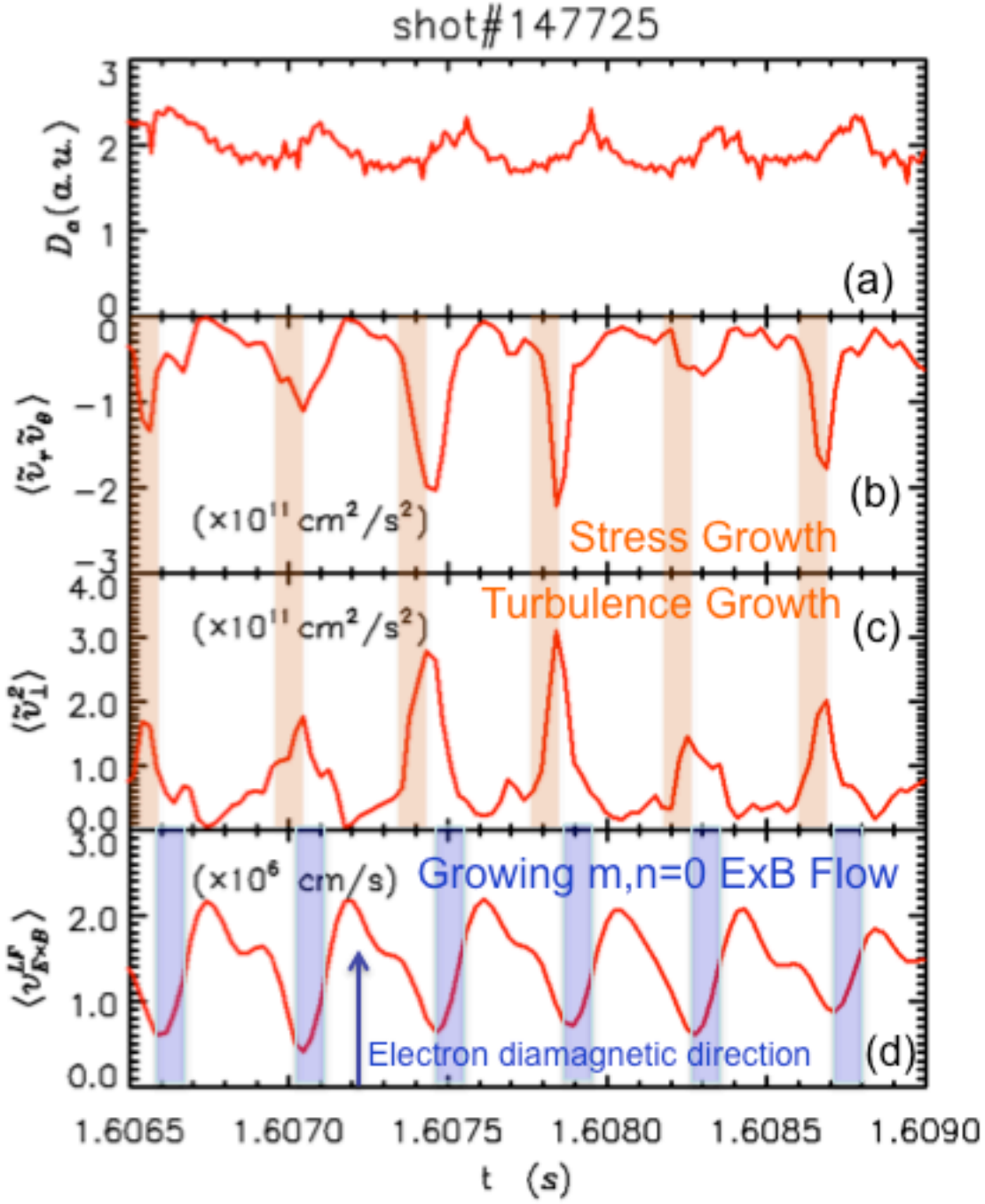

Fig. 4: (a) D_α *light modulations, (b) turbulent stress and (c) turbulent energy, (d): m,n=0 ExB flow velocity. Data taken ~1cm inside LCFS in DIII-D LCO regime.*

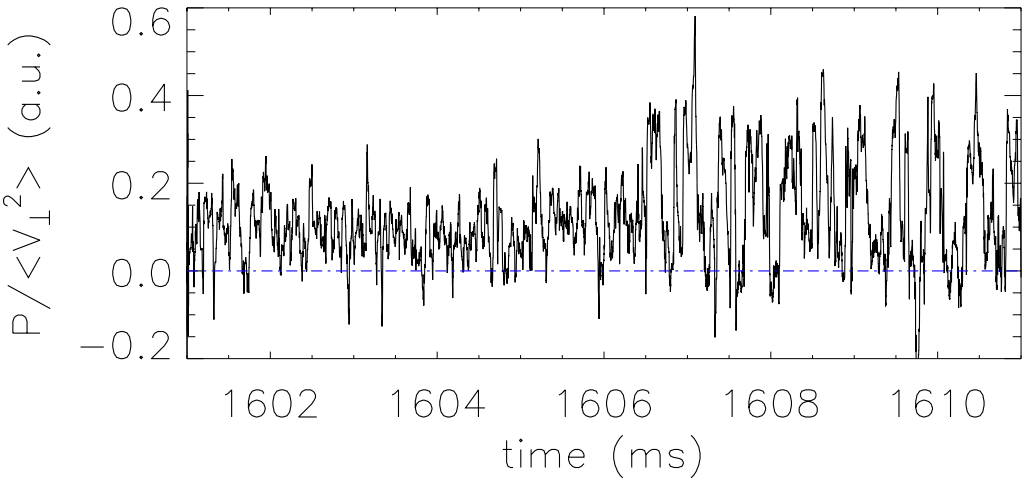

Fig. 5: Nonlinear kinetic energy transfer rate during the transition from L-mode to the LCO regime. Data obtained by velocimetry analysis of DIII-D BES turbulence imaging data of DIII-D shot 147725, centered on region 1cm inside the LCFS. The results show a jump in the relative rate of nonlinear energy transfer to the low frequency m,n=0 sheared ExB flow at~1606.3 msec and then a subsequent modulation in this transfer rate during the LCO regime, in qualitative agreement with probe results.

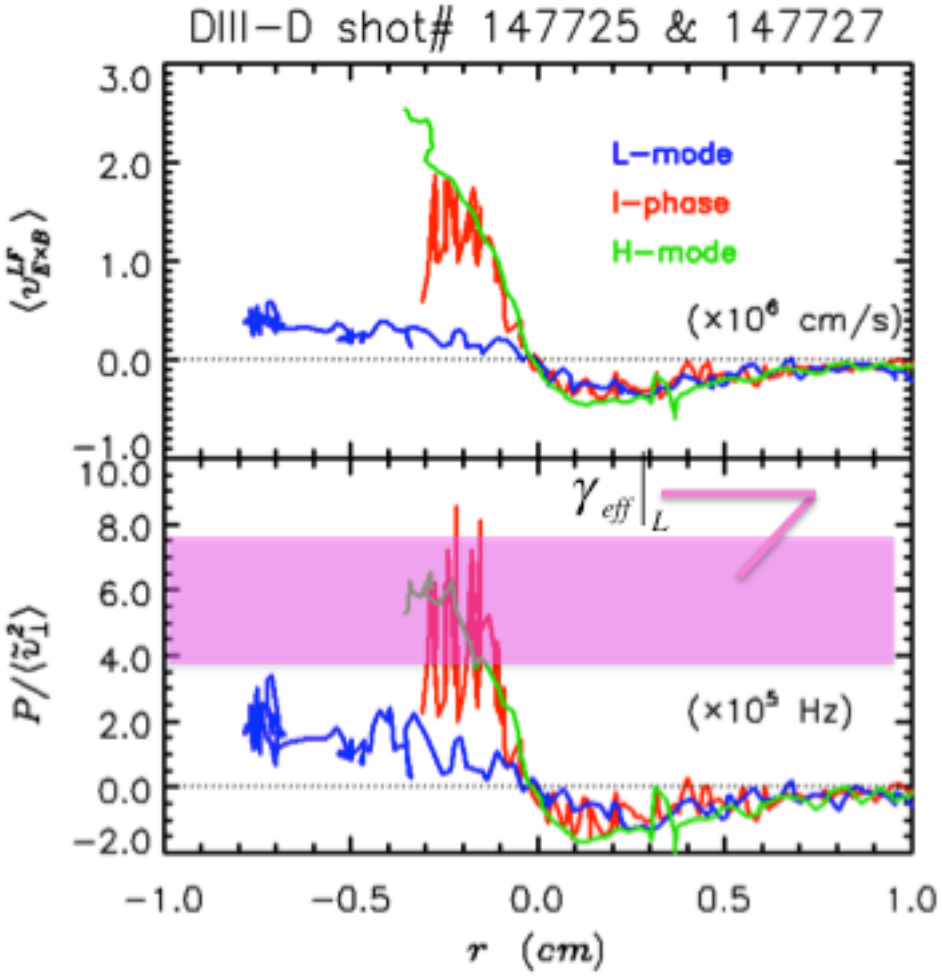

Fig. 6: Top: Radial profiles of low frequency ExB drift profiles in L-mode (blue), Iphase or LCO regime (red) and H-mode (green). Bottom: Radial profiles of normalized energy transfer rate $P_{LF}/\langle\tilde{v}_\perp^2\rangle$ *into the m,n=0 ExB flow in L-mode (blue), LCO or I-phase (red) and H-mode (green), and estimated range of* γ_{eff} *from the preceeding L-mode phase of the discharge.*

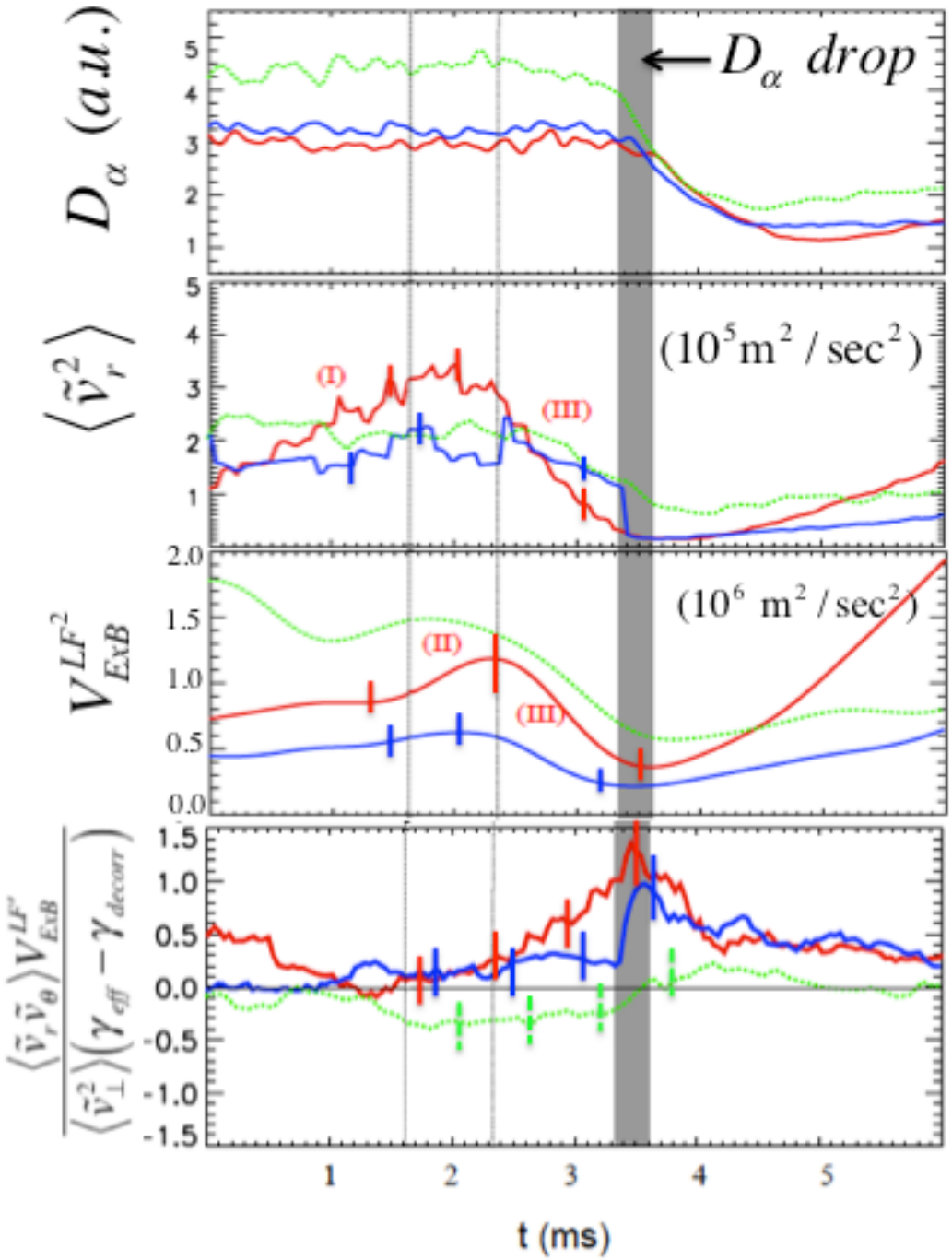

Fig. 7 Top: D_α evolution during EAST L-H transitions. Middle: Turbulent radial kinetic energy and low frequency sheared ExB flow energy. Bottom: Ratio of production, P_{LF} normalized to the effective rate of energy input into the turbulent scale, $P_\perp / v_{net} \langle \tilde{v}^2 \rangle$. Error bars on bottom panel estimated from propagation of random statistical errors. Green line: SOL data. Blue and red: Data obtained ~1cm inside LCFS